Journal of Marine Science and Technology

Volume 23 | Issue 4 Article 13

COUPLING VOF/PLIC AND EMBEDDING METHOD FOR SIMULATING WAVE BREAKING ON A SLOPING BEACH

Tai-Wen Hsu
Department of Habor and River Engineering, National Taiwan Ocean University; Research Center for Ocean Energy and Strategies, Keelung, Taiwan Department of Hydraulic and Ocean Engineering, National Chen Kung University, Tainan, Taiwan, twhsu@mail.ncku.edu.tw

Chih-Min Hsieh
Department of Maritime Information and Technology, National Kaohsiung Marine University, Kaohsiung, Taiwan

Chin-Yen Tsai
Department of Hydraulic and Ocean Engineering, National Chen Kung University, Tainan, Taiwan

Shan-Hwei Ou
Department of Hydraulic and Ocean Engineering, National Chen Kung University, Tainan, Taiwan

Recommended Citation

Hsu, Tai-Wen; Hsieh, Chih-Min; Tsai, Chin-Yen; and Ou, Shan-Hwei (2015) "COUPLING VOF/PLIC AND EMBEDDING METHOD FOR SIMULATING WAVE BREAKING ON A SLOPING BEACH," *Journal of Marine Science and Technology*: Vol. 23: Iss. 4, Article 13.
DOI: 10.6119/JMST-014-1204-2
Available at: https://jmstt.ntou.edu.tw/journal/vol23/iss4/13

COUPLING VOF/PLIC AND EMBEDDING METHOD FOR SIMULATING WAVE BREAKING ON A SLOPING BEACH

Acknowledgements

This research was supported by the National Science Council and the Landmark Project of National Cheng-Kung University, Taiwan, under the Grants No. NSC-96-2221-E127-006-MY3 and A0162.

Journal of Marine Science and Technology, Vol. 23, No. 4, pp. 498-507 (2015)
DOI: 10.6119/JMST-014-1204-2

COUPLING VOF/PLIC AND EMBEDDING METHOD FOR SIMULATING WAVE BREAKING ON A SLOPING BEACH

Tai-Wen Hsu[1, 3], Chih-Min Hsieh[2], Chin-Yen Tsai[3], and Shan-Hwei Ou[3]

Key words: spilling breaker, VOF/PLIC, embedding method, wave breaking.

ABSTRACT

A 2-D numerical model was developed to simulate wave breaking on a sloping beach. The model solves the Reynolds Averaged Navier-Stokes (RANS) equations coupled with the k-ε turbulence closure model. To track free surface configurations, the volume of fluid with piecewise linear interface calculation (VOF/PLIC) is employed. An embedding method (EB) is also used to treat complex bottom topography. Coupling these two methods for simulating wave breaking on a sloping beach, good agreement between numerical results and laboratory observations is found for spilling breaker. Wave breaking characteristics is in terms of free surface profiles, mean velocities and wave heights based on the numerical results. Turbulence transports under wave breaking were also investigated.

I. INTRODUCTION

When waves traveling over a sloping beach and enter water that is approximately as deep as the wave height, they become unstable and then break. Much of the energy is dissipated after wave breaking in the nearshore that provides natural forces to generate nearshore currents. These currents are of great importance in that they combine with waves to transport beach sediment and are a significant factor in controlling the morphology of the beach. In addition, turbulence induced by breaking waves could cause wide spreading of the diffusion processes for suspended particles. Therefore, it is desirable to study the processes of wave energy dissipation in the surf zone which include wave height decay, the movement of bores, wave-induced setup and setdown and longshore current as well as rip current.

In the past few years, due to the advance of computing technology, the numerical wave tank (NWT) has been widely applied in simulating wave breaking. Currently, there are four basic types of numerical models have been used to simulate wave breaking of water waves: (1) non-linear shallow water wave equation, (2) Boussinesq type models, (3) Laplace equation, and (4) Navier-Stokes equations. The first three approaches are based on potential flow, while the last approach is categorized into real flow. For example, Zelt (1991) developed the Boussinesq-type equations in Lagrangian form to simulate wave run-up of nonbreaking and breaking solitary waves. A numerical model was developed by Kobayashi et al. (1987) on the basis of the finite amplitude shallow-water equations to predict wave reflection and runup on rough slopes.

However, the inviscid wave model may fail to capture important phenomena regarding the interaction of viscous fluids with solid structures. So far, only a few numerical models have been proposed for simulating breaking waves travelling over a slopping beach. To study the process of viscous flow interacting with submerged breakwaters, the Navier-Stokes equations with fully nonlinear free surface boundary conditions are considered in this study.

The present stage of using Navier-Stokes equations to simulate breaking waves can be classified into three categories (Zhao et al., 2004): (1) direct numerical simulation (DNS) of Navier-Stokes equations containing turbulent flow (Petit et al., 1994); (2) numerical solution of the Reynolds-Averaged Navier-Stokes (RANS) equations (Lemos, 1992; Lin and Liu. 1998a, 1998b; Hsiao and Lin, 2010; Xie, 2013; Xie, 2014); and (3) numerical solution of the space-filtered Navier-Stokes equations (Zhao and Tanimoto, 1998; Christensen and Deigaard, 2001; Zhao et al., 2004; Lubin et al., 2006; Lakehal and Liovic, 2011; Lubin et al., 2011). Among them, DNS demanding a sufficiently refined grid size to account for all the length-scales of the turbulent flow is too computationally expensive to apply in a large coastal waters. The space-

Paper submitted 05/18/14; revised 10/27/14; accepted 12/04/14. Author for correspondence: Tai-Wen Hsu (e-mail: twhsu@mail.ncku.edu.tw).
[1] *Department of Habor and River Engineering, National Taiwan Ocean University; Research Center for Ocean Energy and Strategies, Keelung, Taiwan, R.O.C.*
[2] *Department of Maritime Information and Technology, National Kaohsiung Marine University, Kaohsiung, Taiwan, R.O.C.*
[3] *Department of Hydraulic and Ocean Engineering, National Chen Kung University, Tainan, Taiwan, R.O.C.*

filtered method uses a cell volume filter to describe the subgrid turbulence in which the Smagorinsky subgrid scale (SGS) Reynolds stress and large eddy scale (LES) are implemented in the model. Although SGS model shows remarkable results of breaking waves, however, the computations are very laborious and time consuming. Instead, the RANS model coupled with turbulence closure models are commonly used to simulate the evolution of breaking waves of kinematics and turbulence in the surf zone. It has the advantage of computational efficiency and reliability to simulate wave breaking processes.

Based on the review given above, progress in developing a numerical model for wave breaking processes on a sloping beach has been steadily performed. Gueyffier et al. (1999) developed volume of fluid (VOF) method to a second-order accuracy. Tsai et al. (2008) applied this technique to simulate spilling breaker travelling over a sloping beach. In this paper the VOF method using piecewise linear interface calculation (PLIC), designated as VOF/PLIC, has been employed to track the free surface. In the model, a Lagragian advection is used to advent the interface segments and calculate the corresponding volume flux in the cell. The wall boundary condition is described by the embedding (EB) method developed by Ravoux et al. (2003), in which the solid boundary is accounted for by adding a force field to the flow phase in the computed cells that are fully or partially occupied by the solid phase. Therefore, there is no need to impose boundary conditions on the body surface since the velocity components are made vanish within the bodies as a part of the solution. A 2D numerical model was developed to predict flow characteristics on a sloping beach for spilling breaker. The boundary conditions were improved based on VOF/PLIC and EB. The model is extensively examined with the experimental data for a train of waves breaking over sloping beaches. Flow characteristics of wave breaking propagation over sloping profiles is presented and discussed. Numerical results are in terms of the free surface profiles, the mean velocities, the turbulent kinetic energies and the eddy viscosities.

II. MODEL DESCRIPTION

1. Governing Equations

Waves propagating over a sloping beach is considered in this investigation. The Cartesian coordinate system is utilized as shown in Fig. 1, where h is the quiescent water depth in front of a sloping beach, H_0 is the incident wave height. The RANS model developed by Lin and Liu (1998a; 1998b) is widely used for solving ocean problems. This model solves 2D RANS equations for the mean flow field combined with the k-ε turbulence closure. The governing equations which describe the mean quantities of the flow field for unsteady incompressible turbulent flows are the Reynolds-averaged equations consisting of the continuity equation for incompressible flow and momentum equations written as follows,

Continuity equation:

$$\frac{\partial U}{\partial x}+\frac{\partial W}{\partial z}=0\,, \tag{1}$$

Momentum equation:

$$\frac{\partial U}{\partial t}+U\frac{\partial U}{\partial x}+W\frac{\partial U}{\partial z}=-\frac{\partial P}{\partial x}+(\nu_t+\nu)\nabla^2 U + \frac{\partial}{\partial x}(\nu_t\frac{\partial U}{\partial x})+\frac{\partial}{\partial z}(\nu_t\frac{\partial W}{\partial x})-\frac{2}{3}\frac{\partial k}{\partial x}\,, \tag{2}$$

$$\frac{\partial W}{\partial t}+U\frac{\partial W}{\partial x}+W\frac{\partial W}{\partial z}=-\frac{\partial P}{\partial z}+(\nu_t+\nu)\nabla^2 W + \frac{\partial}{\partial x}(\nu_t\frac{\partial U}{\partial z})+\frac{\partial}{\partial z}(\nu_t\frac{\partial W}{\partial z})-\frac{2}{3}\frac{\partial k}{\partial z}-g, \tag{3}$$

where x and z are the horizontal and vertical coordinates in a fixed Cartesian system, t is the time, U and W are the mean velocity components in the x- and z-directions, P is the pressure, g is the gravitational acceleration, ν_t is the eddy viscosity, ν is the molecular viscosity, $\nabla=(\partial/\partial x,\ \partial/\partial y)$ is the gradient operator, and k is the turbulent kinetic energy.

The Reynolds stress closure model is the k-ε model for resolving the eddy viscosity in the present study. The eddy viscosity is represented by the turbulent kinetic energy k and energy dissipation rate ε using the Boussinesq assumption, that is

$$\nu_t=\frac{C_\mu k^2}{\varepsilon}\,, \tag{4}$$

The transport equations of the turbulent kinetic equation (TKE) and energy dissipation equation (EDE) are used as the closure equations:

$$\frac{\partial k}{\partial t}+U\frac{\partial k}{\partial x}+W\frac{\partial k}{\partial z}=\nabla\cdot\left[\left(\nu+\frac{\nu_t}{\sigma_k}\right)\nabla k\right]+Prod-\varepsilon\,, \tag{5}$$

$$\frac{\partial \varepsilon}{\partial t}+U\frac{\partial \varepsilon}{\partial x}+W\frac{\partial \varepsilon}{\partial z}=\nabla\cdot\left[\left(\nu+\frac{\nu_t}{\sigma_\varepsilon}\right)\nabla \varepsilon\right] + C_l\nu_t\frac{\varepsilon}{k}Prod-C_2\frac{\varepsilon^2}{k}\,, \tag{6}$$

where *Prod* term represents the production of turbulent kinetic energy expressed as

$$Prod=\nu_t\left[2\left(\frac{\partial U}{\partial x}\right)^2+2\left(\frac{\partial W}{\partial z}\right)^2+\left(\frac{\partial U}{\partial z}+\frac{\partial W}{\partial x}\right)^2\right], \tag{7}$$

where σ_k, σ_ε, C_μ, C_1 and C_2 are empirical coefficients and are taken to be $\sigma_k = 1.0$, $\sigma_\varepsilon = 1.3$, $C_u = 0.09$, $C_1 = 1.44$ and $C_2 = 1.92$ as suggested by Rodi (1980) and Hsu et al. (2004).

2. Initial and Boundary Conditions

The initial condition and boundary conditions are specified to solve the boundary value problems. At the beginning of the flow simulation the velocity components U and W are both set to zero throughout the whole flow field. The hydrostatic pressure is utilized for the first stage of the pressure field.

For the turbulence quantities field, the logarithmic distribution of mean tangential velocity in the turbulent boundary layer is applied, where the values of k and ε are assumed as functions of distance from the boundary and the mean velocity outside the viscous layer. On the free surface, the zero-gradient boundary conditions are imposed for both k and ε, i.e. $\partial k/\partial n = 0$ and $\partial \varepsilon/\partial n = 0$ (Launder, 1989). The specification of inflow boundary conditions require more careful treatments to avoid singular terms existing in the EDE when $k = 0$. Following Lin and Liu (1998a), it is necessary to seed a small amount of k as the initial disturbance. The initial value is imposed by setting $k = U_p^2/2$, where $U_p = A_1 C_p$, U_p and C_p are the horizontal mean velocity and wave celerity on the upstream boundary. The value of A_1 is somewhat arbitrary and is taken to be 2.5×10^{-3} as suggested by Lin and Liu (1998a; 1998b).

Four boundary conditions are considered in this study, including the upstream, downstream, free surface and solid boundaries. In the numerical computations the free-surface displacements and the velocity components of two kinds of periodic waves are given as the inflow conditions at the upstream end. The first kind of periodic wave is selected as the co-sinusoidal wave based on linear wave theory. The other incident wave is the Cnoidal (Cn) wave which is a nonlinear wave profile. The wave profile reads (Isobe et al., 1987)

$$h_s = h + \eta = h \sum_{n=0}^{3} A_n \mathrm{cn}^{2n}\left[2\kappa\left(\frac{x}{L} - \frac{t}{T}\right)\right], \tag{8}$$

where $\kappa = 2\pi/L$ is the wavenumber and L is the wavelength. The horizontal and vertical velocity components are given by

$$U = \sqrt{gh} \sum_{n=0}^{3}\sum_{m=0}^{2} B_{nm}\left(\frac{h+z}{h}\right)^{2m} \mathrm{cn}^{2n}\left[2\kappa\left(\frac{x}{L} - \frac{t}{T}\right)\right], \tag{9}$$

$$W = \sqrt{gh} \cdot \mathrm{sn}\left[2\kappa\left(\frac{x}{L} - \frac{t}{T}\right)\right] \cdot \mathrm{dn}\left[2\kappa\left(\frac{x}{L} - \frac{t}{T}\right)\right] \times \frac{4\kappa h}{L} \sum_{n=1}^{3}\sum_{m=1}^{2} \frac{n}{2m+1} B_{nm}\left(\frac{h+z}{h}\right)^{2m+1} \cdot \mathrm{cn}^{2n}\left[2\kappa\left(\frac{x}{L} - \frac{t}{T}\right)\right], \tag{10}$$

where A_n and B_{nm} in Eqs. (8) to (10) are coefficients determined based on the theory of Isobe et al. (1987); cn, sn, and dn are Jacobian elliptic functions, respectively.

The non-slip boundary conditions is applied on the solid boundary for the mean flow field. On the free surface boundary, one kinetic and two dynamic boundary conditions are used which are written in the form,

$$\frac{\partial h_s}{\partial t} + U\frac{\partial h_s}{\partial x} = W, \text{ at } z = h_s(x,t), \tag{11}$$

$$\mu\left(\frac{\partial U_\tau}{\partial n} + \frac{\partial U_n}{\partial \tau}\right) = S_\tau, \text{ at } z = h_s(x,t), \tag{12}$$

$$-P + 2\mu\frac{\partial U_n}{\partial n} = S_n, \text{ at } z = h_s(x,t), \tag{13}$$

where the subscripts n and τ denote the outward normal and tangential directions, respectively.

3. Interface Calculation

Like other studies of free surface flows, we also encounter difficulties in treating the free surface boundary conditions of wave breaking on a sloping beach. A suitable way of finding the free surface is of great importance in the numerical calculation. The piecewise linear interface calculation (PLIC) method presented by Gueyffier et al. (1999) which was developed on the basis of VOF is adopted in this study to track the rapidly varying water surfaces during wave breaking. The VOF/PLIC is expanded to the second-order in order to treat the interface with Lagrangian advection of the interface more precisely. This method was first implemented in Tsai et al. (2008) computation of wave breaking on a sloping beach.

Based on Hirt and Nichols (1981), we define a VOF function, $F(x, z, t)$, which represents the fractional volume of fluid occupied on every cell, which is described by the following equation

$$\frac{\partial F}{\partial t} + U\frac{\partial F}{\partial x} + W\frac{\partial F}{\partial z} = 0, \tag{14}$$

As mentioned above the algorithm of VOF/PLIC by Gueyffier et al. (1999) is used for describing water surface configuration with higher-order accuracy. The procedure for this algorithm is divided into two steps: a reconstruction step and a propagation step. The first step is the determination of the orientation of the segment and the area occupied by water in a surface cell with the known volume fraction F. For the second step, a Lagragian advection technique is utilized to advect the interface segments and evaluate the corresponding volume fluxes in the fluid cell.

For the solid boundary condition, a flexible immersed boundary method was proposed by Peskin and Printz (1993) to enforce no-flow boundary conditions on the boundary using discrete delta functions on boundaries. However, it has been

shown to lose accuracy in rigid boundaries (Lai and Peskin, 2000). The other alternative is the embedding (EB) method developed by Ravoux et al. (2003). The model represents the solid body by adding a force field to the fluid momentum equations in the computational cells that are fully or partial occupied by the solid phase. Details of the EB method are referred to Ravoux et al. (2003). An advantage of the EB method is that the computations are performed on a Cartesian grid without the need to fit the complex boundaries. For this reason, EB is first applied in the present investigation to simulate wave breaking and energy decay on a sloping beach. We rewrite the momentum equations by adding the virtual force term as follows.

$$\frac{\partial U}{\partial t} = Rhs_x + f_x , \tag{15}$$

$$\frac{\partial W}{\partial t} = Rhs_z + f_z , \tag{16}$$

where f_x and f_z are the horizontal and vertical direction virtual force/body force terms. Rhs_x and Rhs_z are the horizontal and vertical direction convective and diffusive terms of the momentum equations, respectively.

The three-step time-split scheme is used to advance the flow field. First the velocity is stepped from the nth time level to the first intermediate level "*" by solving the advection-diffusion equations without the pressure and virtual force for the momentum equation. Subsequently, this step can be written in the forms

$$\frac{U^* - U^n}{\Delta t} = {Rhs_x}^n , \tag{17}$$

$$\frac{W^* - W^n}{\Delta t} = {Rhs_z}^n , \tag{18}$$

At this stage, one treats the system as a "binary" fluid. One phase is simply the ordinary fluid outside the rigid body while the other is the structure phase itself, within the velocity is expected to vanish. To exactly identify the cells assigned to each phase, a volume fraction field is defined as the fraction of the area of each cell occupied by the structure. By imposing the body force term (f_x, f_z) in those cells that are partially or fully occupied by the structure, we modify the velocity field to make it vanish in the structure. Namely, the presence of the body force in the x-and z-momentum equation implies the update equation, respectively,

$$\frac{U^{**} - U^*}{\Delta t} = f_x , \tag{19}$$

$$\frac{W^{**} - W^*}{\Delta t} = f_z , \tag{20}$$

where U^* and U^{**} are intermediate value of the velocity before and after this fraction step. The embedding method determines the force f_x to make the update velocity U^{**} vanish within the structure. To make the velocity vanish inside the structure but remain unchanged in the fluid, the case of the velocity component (U, W), We set

$$U^{**} = U^* + f_x \Delta t = U^* + \Phi_x \frac{(-U^*)}{\Delta t} \Delta t = (1 - \Phi_x) U^* , \tag{21}$$

$$W^{**} = W^* + f_z \Delta t = W^* + \Phi_z \frac{(-W^*)}{\Delta t} \Delta t = (1 - \Phi_z) W^* , \tag{22}$$

where Φ_x and Φ_z are the fractional volume of structure, i.e.

$$\Phi(x,z) = \begin{cases} 1 & \text{inside the structure} \\ 0 \sim 1, & \text{on the structure surface} \\ 0 & \text{in the flow domain} \end{cases} , \tag{23}$$

Thus, in cell (i,k) inside the structure, the velocity along the x-direction is canceled out since $\Phi_x(i,k) = 1$. In the boundary cells, the update velocity is partially modified since $\Phi_x(i,k)$ is between zero and one. Outside the structure $\Phi_x(i,k) = 0$ and $U^{**}(i,k)$ is identical to $U^*(i,k)$ so that the flow remains unchanged. By inserting Eq. (21) into Eq. (19), the value of the body force in the horizontal direction is deduced:

$$f_x(i,k) = \frac{-\Phi_x(i,k) \cdot U^*(i,k)}{\Delta t} \Delta t , \tag{24}$$

Substituting Eq. (22) into Eq. (20), the value of the body force in the vertical direction is deduced:

$$f_z(i,k) = \frac{-\Phi_z(i,k) \cdot W^*(i,k)}{\Delta t} \Delta t , \tag{25}$$

Following Hsu et al. (2004), the RANS equations were solved numerically by a finite volume method with a staggered system. Velocity components are defined at the midpoints of a cell face to ensure mass conservation, the pressure, the turbulent kinetic energy, the dissipation rate of energy and the wave profile are defined at the center of the cells. For a detailed description of the numerical procedure, the readers may refer to Hsu et al. (2004).

In order to achieve the numerical stability and accuracy, appropriate mesh increments Δx, Δz and Δt must be selected in the standard finite difference approximation of VOF method. For accuracy, the grid sizes should be chosen small enough to resolve the temporal and spatial variations of all flow characteristics. However, the VOF/PLIC combined with EB method provide flexibly larger grid sizes to raise numerical efficiency.

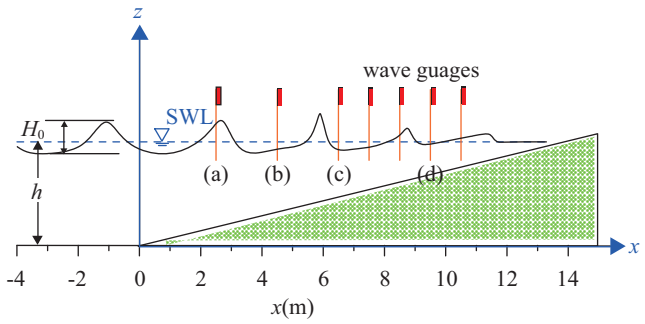

Fig. 1. Definition diagram of periodic wave train over a sloping bed. (a), (b), (c) and (d) denote four locations for measuring temporal variations of water surface elevations for waves travelling over a sloping beach.

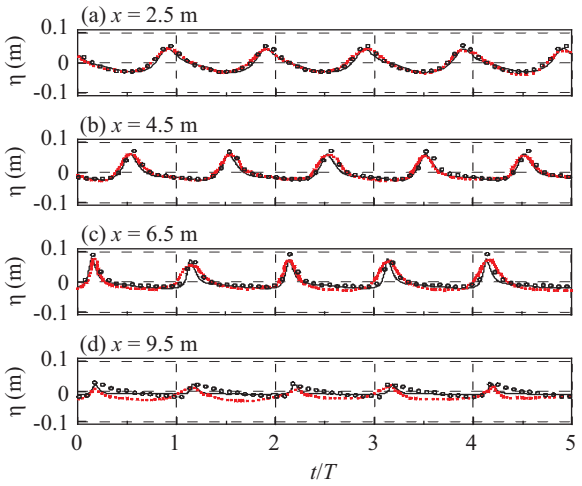

Fig. 2. Comparisons of simulated (solid line) and measured (open circles, Ting and Kirby (1994) water surface elevations at the shoaling regions (a)-(c) and the bore region (d).

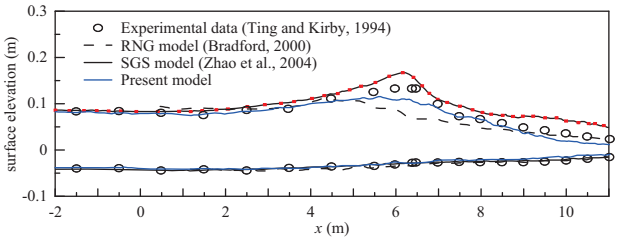

Fig. 3. Computed and measured spatial distribution of wave crest elevations and wave trough depressions of the spilling breaker.

III. VERIFICATIONS

Numerical simulations of breaking waves on a sloping beach are conducted to evaluate the performance of the present model. For the comparison with the other models, experimental data sets were used to compare with numerical results.

Fig. 1 shows the schematic sketch of waves propagating over a sloping beach, where the beginning of the sloping bed is located at x = 0 m. Ting and Kirby (1994) performed experiments to investigate the evolution of a spilling breaker of Cn wave over a sloping bed. The incident wave height and period are H_0 = 0.125 m and wave period T = 2.0 s with a constant water depth of 0.4 m for waves propagating a sloping beach. Wave breaking occurs at breaking point x = 6.4 m with a spilling breaker on a 1/35 slope. The temporal variation of water surface elevations were measured at 4 various locations (a)~(d) (see Fig. 1) over the bed. In the numerical simulation, the computational domain is 28 m long and 0.4 m high with the grid sizes Δx = 0.02 m and Δz = 0.0075 m in VOF method, and minimum grid sizes Δx = 0.02 m, Δz = 0.01 m in VOF/PLIC together with EB method. The simulations were conducted for 60 s of waves.

Fig. 2 shows comparison of the simulated and measured instantaneous water surface elevations from the shoaling region to the bore region. It is noted that the model results agree very well with the experimental measurements. Note that the VOF/PLIC technique used in the present model predicts a better result than the VOF method at the bore region. In Fig. 2, we also notice that the wave profiles presents shorter and higher wave crests and longer and flatter wave troughs after wave breaking. In such condition, much wave energy has been released at the breaking point where wave height suddenly decreases.

Fig. 3 shows comparison of the computed and measured wave crest elevations and trough depressions with Ting and Kirby's data, where in numerical results given by Bradford's (2000) RNG model and Zhao et al.'s (2004) SGS model are also plotted for comparison. It is seen that the predicated wave crest profile by the present model agrees well with experiments except for the values in the region x = 5.5~6.4 m. In this case, the wave breaking point occurs at x = 6.4 m and the bore region happens between x = 7.5 m and x = 9.11 m. The computed breaking point by the present model is located at x_b = 6.1 m, which is very close to the measured breaking point. Notably, the RNG model predicts the wave breaking far early than that observed in the experiment, and also underestimates the wave crests in the surf zone. The computed breaking point by SGS model is at x = 6.16 m, which is also very close to the observed breaking point. However, the model also overestimates surface elevations near the breaking point as well as in the bore region. This result indicates that the VOF/PLIC could improve numerical schemes for describing the water surface profile with higher-order accuracy. The present model accurately predicts the wave height at the inner surf zone in that the surface profile presents a more peaked crest and flatter trough.

The phase averaged horizontal and vertical velocities compared with laboratory measurements are shown in Fig. 4. At the region of the wave breaking and the surf zone comparisons are made at two locations of x = 7.275 m and 9.11 m at different vertical locations z = -0.1 m, -0.06 m and -0.02 m. The general agreement between the simulated results and measured data is good for SGS and the present model. However, it seems that the accuracy of the present model is

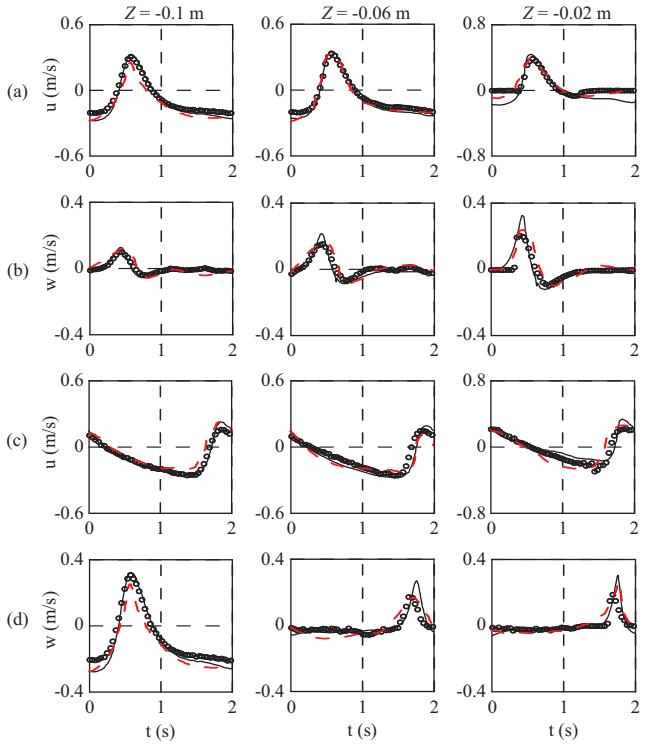

Fig. 4. Comparisons of phase averaged horizontal and vertical velocities at initial breaking x = 7.275 m (a), (b) and bore region x = 9.110 m (c), (d). The vertical locations are, from left to right, z = -0.10; -0.06; -0.02 m. Lines: the present model; circles: experimental data from Ting and Kirby (1994); solid lines: present model; dash lines: SGS model of Zhao et al. (2004).

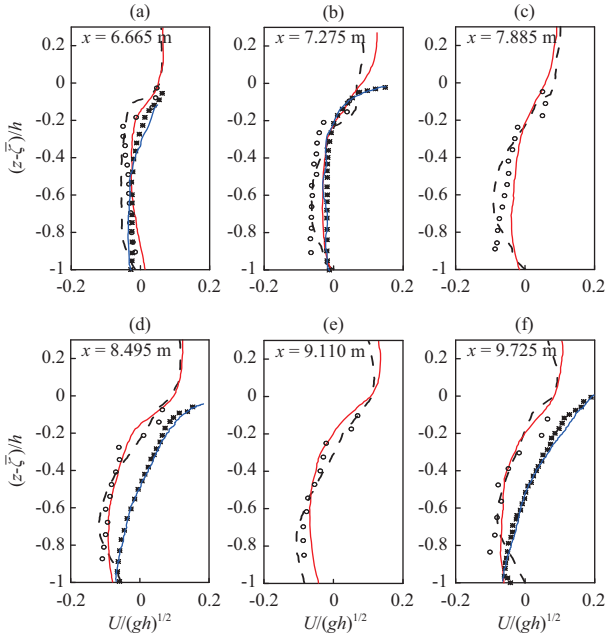

Fig. 5. Comparisons of simulated and measured undertows. Solid line: present model; dashed lines: SGS model (Zhao et al., 2004); solid cross line (Bradford, 2000); open circles: experimental data from Ting and Kirby (1994). From (a) to (f) at locations x = 6.665; 7.275; 7.885; 8.495; 9.110; 9.725 m.

better than SGS towards the free surface. This is mainly due to the fact that numerical resolution of VOF/PLIC on the surface is higher.

Zhao et al. (2004) showed that the wall boundary condition needs to be implemented to get accurate undertow profiles. Here the EB method described by Ravoux et al. (2003) is used. Fig. 5 depicts the computed and measured undertow profiles at six different measured locations. Notably the present model reproduces the experimental data favorable in which the magnitude and profile shape are well represented. The RNG model in general seems to underestimate the undertow and fails to predict the undertow profile. The SGS model shows general agreement between numerical and experimental results. However, we note that the SGS model overestimates the undertow profile at four locations shown in Figs. 5(b), (c), (d) and (f). This comparison indicates that the accuracy of the RANS model seems to be significantly improved for the prediction of undertow using EB method to the spilling breaker case.

IV. RESULTS AND DISCUSSION

In this section, we present numerical results and make some discussion on mean flow field and turbulent transport mechanism under wave breaking on a sloping bottom using the present model. Interesting issues are physical property induced by a spilling breaker, including the flow field, normalize vortices, turbulent kinetic intensity, turbulent dissipation and eddy viscosity. Four snapshots at different wave phases, i.e. t/T = 0, 0.25, 0.5 and 0.75, are demonstrated in the spatial domain to give a precise description of some interesting phenomena in the breaking processes.

Fig. 6 displays the spatial variations of the mean flow field. The mean velocity is normalized by the wave celerity $c = \sqrt{gh}$. At t/T = 0, a wave crest just passes the breaking location (x = 6.4 m). It is shown that the roller acts as the recirculating flow in the front of the turbulent bore. A jet is ejected from the crest of the breaking wave and impacts in the very upper part of the face of a wave. In the roller region, the horizontal fluid particle velocity is strong and roughly equal to the local phase velocity. Fig. 7 shows the normalized mean vorticity field $\Omega = \sqrt{gh}$ under the spilling breaker, where $\Omega = (\partial U/\partial z - \partial W/\partial x)$ is the vorticity strength. It is noticed that a vortex starts to form at the toe of the wavefront right before wave breaking. This vortex is further strengthened and convected to almost the whole crest region.

The turbulent intensity is defined as

$$I = \sqrt{(u'u' + w'w')} = \sqrt{2k} \tag{26}$$

where u' and w' are the velocity fluctuations in the x and z direction, respectively. Following Lin and Liu (1998a, 1998b), the turbulence intensity is normalized by wave celerity c =

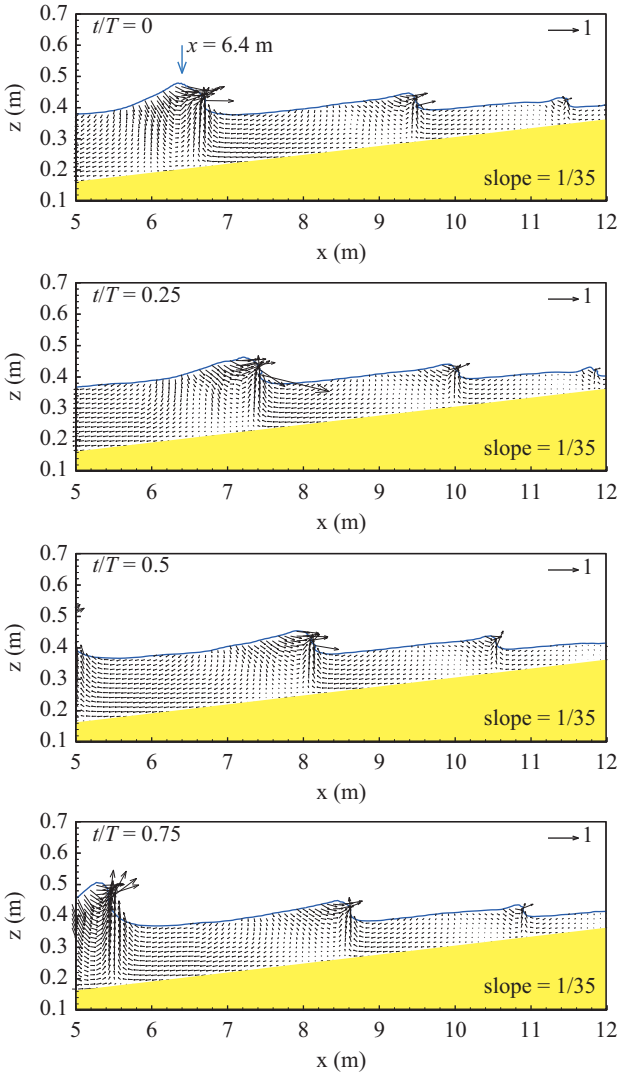

Fig. 6. Simulated velocity fields for spilling wave breaker over a sloping beach at different wave phases. (a) $t/T = 0$; (b) $t/T = 0.25$; (c) $t/T = 0.5$; (d) $t/T = 0.75$. The velocity is normalized by $\sqrt{gh}$.

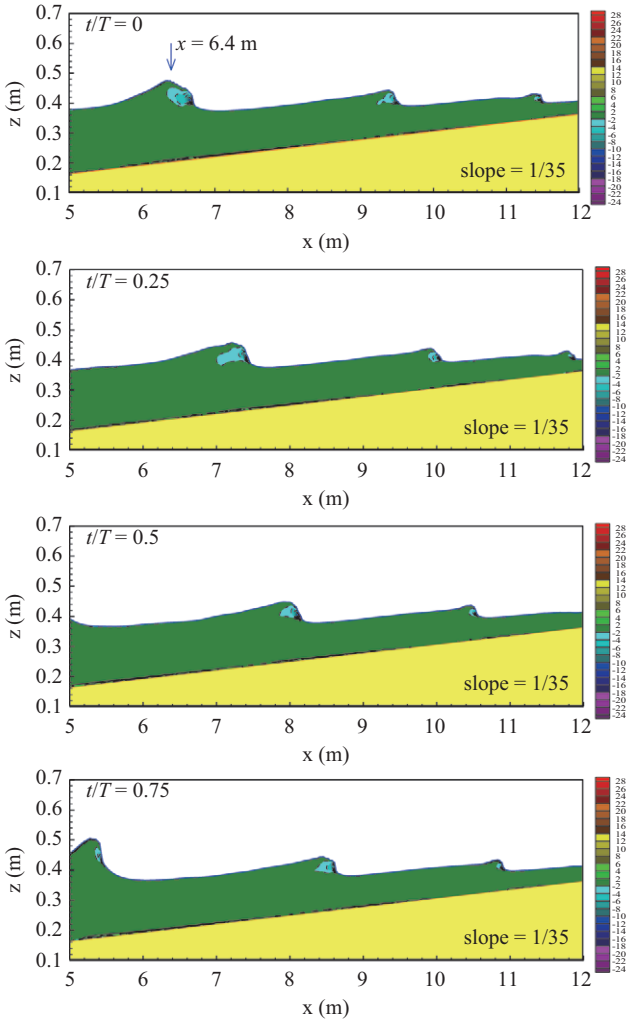

Fig. 7. Simulated normalized vorticity for spilling wave breaker over a sloping beach at different wave phases. (a) $t/T = 0$; (b) $t/T = 0.25$; (c) $t/T = 0.5$; (d) $t/T = 0.75$. The normalized vorticityis $(\partial U/\partial z - \partial W/\partial x)/\sqrt{gh}$.

$\sqrt{gh}$. The snapshots of turbulent intensity are presented in Fig. 8. Fig. 8 shows that the turbulent intensity is generated just before the breaking point and is higher in the roller region and forward to the face of the wave. Under the spilling breaking wave, the turbulent kinetic energy continues to dissipate in the bore region. This is due to the high shear rates at the wave front, which generates significant levels of k at the lower front face of the wave. As the wave propagates forward, the turbulence kinetic energy gradually decreases but with very similar patterns of turbulence distribution. Note that the turbulent intensity is then convected and diffused to the forward face of the wave, remaining in considerable amount as the wave moves into the surf zone.

The turbulent dissipation is presented in Fig. 9. It is seen that the turbulent dissipation takes place above the wave trough and at the wavefront, with no turbulent dissipation under the wave crest. The turbulent dissipation displays a long tail at the back face of the wave when the wave approaches the shore.

The eddy viscosity is an important parameter measuring the mixing rate of momentum. Fig. 10 demonstrates the spatial distribution of the eddy viscosity. The eddy viscosity has been normalized by the molecular viscosity. The eddy viscosity decreases with the shoaling of water depth after wave breaking. Since the eddy viscosity is proportional to the length scale and turbulent intensity. When compared with the turbulent intensity, the eddy viscosity decreases faster in the surf zone. It is noted that mean vorticity, turbulent intensity, turbulent dissipation, and eddy viscosity are mainly concentrated in the region very close to breaking wave fronts. In other regions, these four quantities are rather small, which suggests that the mean flow is almost a potential flow with little influence from the breaking processes.

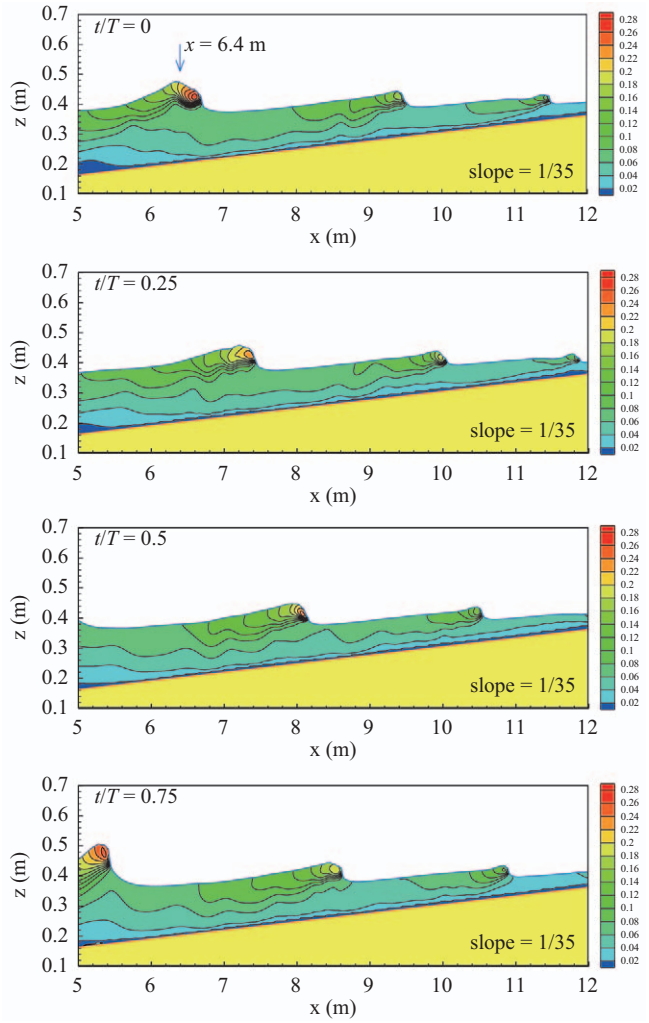

Fig. 8. Simulated normalized turbulent intensity $(2k)^{1/2}/(gh)^{1/2}$ for spilling wave breaker over a sloping beach at different wave phases. (a) $t/T = 0$; (b) $t/T = 0.25$; (c) $t/T = 0.5$; (d) $t/T = 0.75$.

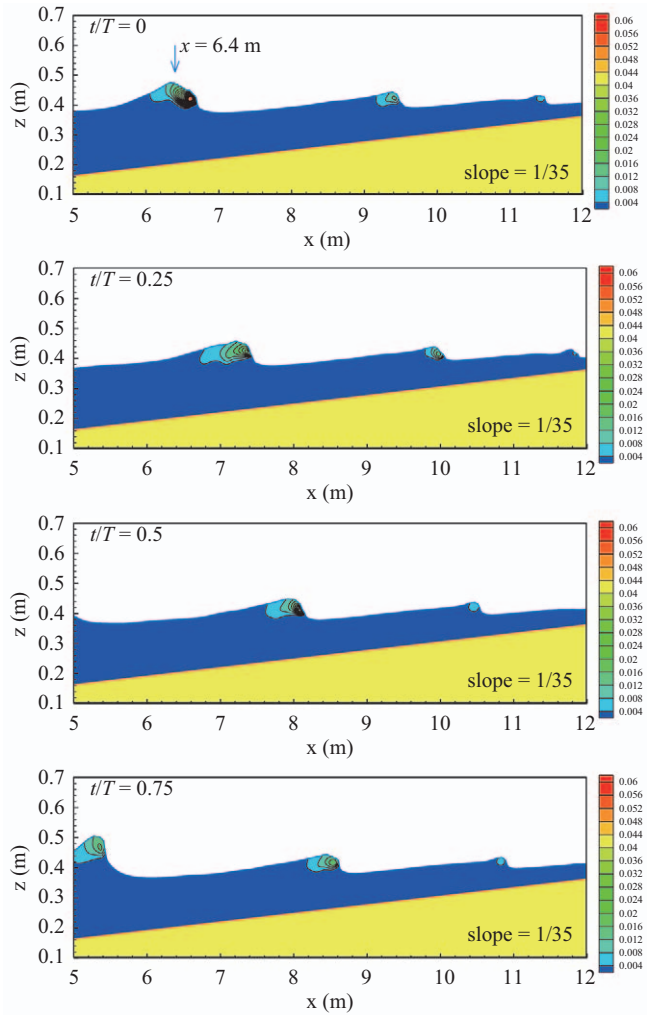

Fig. 9. Simulated normalized turbulent dissipation for spilling wave breaker over a sloping beach at different wave phases. (a) $t/T = 0$; (b) $t/T = 0.25$; (c) $t/T = 0.5$; (d) $t/T = 0.75$. The normalized turbulent dissipation is $\varepsilon/g(gh)^{1/2}$.

V. CONCLUDING REMARKS

A two-dimensional turbulent model was developed to simulate spilling wave breaker in the surf zone by directly solving Reynolds Averaged Navier-Stokes (RANS) equations and the continuity equation. The VOF with piecewise linear interface calculation (VOF/PLIC) which was developed to a second order accuracy is adopted to track the free surface configurations on a Cartesian grid. On the other hand, the present model is improved on the solid boundary using embedding (EB) method of Ravoux et al. (2003). The complex bottom topography is accounted for using EB in which the solid boundary is represented by adding a force to the flow phase in the computed cells that are fully or partially occupied by the solid phase. The advantage is that it is unnecessary to impose boundary conditions on the body surface. By applying the developed model to the problems of spilling wave breaking on a sloping bottom, we found that the model results compare very well with experimental measurements as well as other RANS model results in which the mesh increment are chosen sufficiently small. Numerical results are in terms of water surface elevations, mean particle velocities, wave height distributions and undertow profiles. In general, the present model showed favorable agreements to the experiments and SGS model results by Zhao et al. (2004). The improvement is especially significant on the free surface and undertow profile near the bottom under the spilling breaker. As noted in section 3, VOF is a step function that is still needed to choose small enough to resolve the temporal and spatial variations of flow characteristics for wave breaking. However, the present model could provide a flexible course grid system to lower computational expense for the breaking wave problem.

Detailed analysis of numerical results also showed that the turbulent intensity and vorticity are primarily located above the wave trough. The turbulent intensity is convected and diffused to the forward face of the wave, and continues to

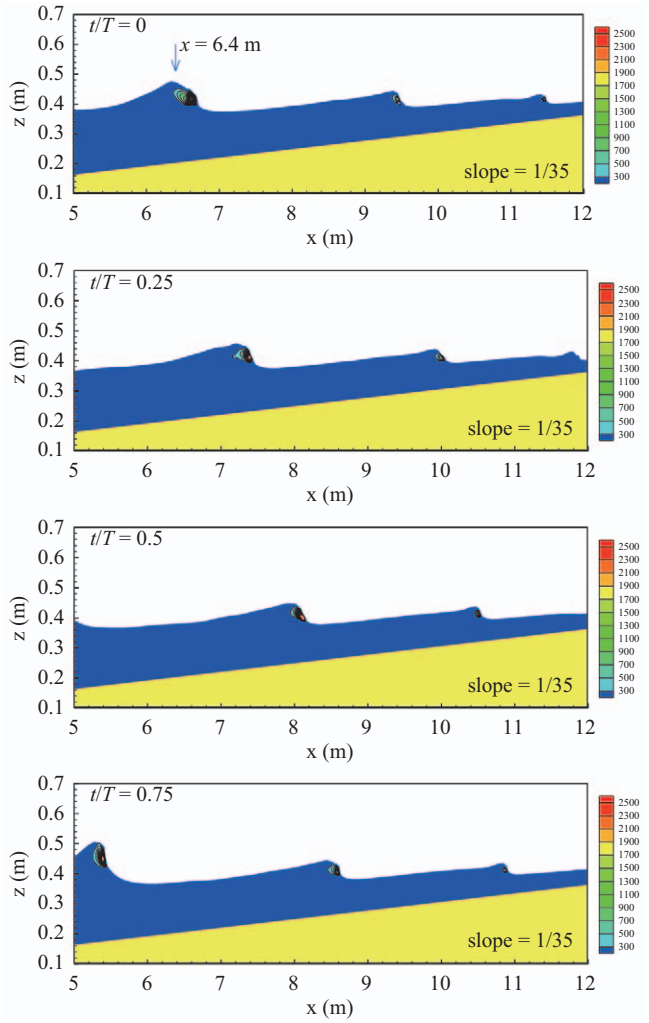

Fig. 10. Simulated normalized eddy viscosity for spilling wave breaker over a sloping beach at different wave phases. (a) $t/T = 0$; (b) $t/T = 0.25$; (c) $t/T = 0.5$; (d) $t/T = 0.75$. The eddy viscosity is normalized by molecular viscosity ν_t/ν.

dissipate while the breaking wave moves towards the shore. After the recovery of wave energy, the second wave breaking takes place and the vorticity in the bore region is larger than that in other regions. The eddy viscosity shows the same pattern of the turbulent intensity between the breaking and role region.

The numerical model accurately reproduces the wave breaking, the recovery and the complicated dynamics generated under spilling breaking waves. A detailed description is provided in terms of free surface, velocity field, and turbulent energy transport. Future study on numerical simulations of the plunging breaker is undertaken and will be reported.

ACKNOWLEDGMENTS

This research was supported by the National Science Council and the Landmark Project of National Cheng-Kung University, Taiwan, under the Grants No. NSC-96-2221-E-127-006-MY3 and A0162.

REFERENCES

Bradford, S. F. (2000). Numerical simulation of surf zone dynamics. Journal of Waterway, Port, Coastal and Ocean Engineering, ASCE 126, 1-13.

Christensen, E. D. and R. Deigaard (2001). Large eddy simulation of breaking waves. Coastal Engineering 42, 53-86.

Gueyffier, D., J. Li, A. Nadim, R. Scardovelli and S. Zaleski (1999). Volume-of-fluid interface tracking with smoothed surface stress methods for three-dimensional flows. Journal of Computational Physics 152, 423-456.

Hirt, C. W. and B. D. Nichols (1981). Volume of fluid (VOF) method for dynamics of free boundaries. Journal of Computational Physics 39, 201-225.

Hsiao, S. C. and T. C. Lin (2010). Tsunami-like solitary waves impinging and overtopping an impermeable seawall: experiment and RANS modeling. Coastal Engineering 57(1), 1-18.

Hsu, T. W., C. M. Hsieh and R. R. Hwang (2004). Using RANS to simulate vortex generation and dissipation around impermeable submerged double breakwaters. Coastal Engineering 51, 557-579.

Isobe, M., H. Nishimura and K. Horikawa (1987). Expressions of perturbation solutions for conservative waves by using wave height. Proceeding of the 33rd Annual Conference, JSCE, Japan, 760-761.

Kobayashi, N., A. K. Otta and I. Roy (1987). Wave reflection and run-up on rough slopes. Journal of Waterway, Port, Coastal and Ocean Engineering, ASCE 113(3), 282-298.

Lai, M. C. and C. S. Peskin (2000). An immersed boundary method with formal second-order accuracy and reduced numerical viscosity. Journal of Computational Physics 160, 705-719.

Lakehal, D. and P. Liovic (2011). Turbulence structure and interaction with steep breaking waves. Journal of Fluid Mechanics 674, 522-577.

Launder, B. E. (1989). Second-moment closure and its use in modeling turbulent industrial flows. International Journal for Numerical Methods in Fluids 9, 963-985.

Lemos, C. M. (1992). Wave Breaking, Springer.

Lin, P. and P. L. F. Liu (1998a). A numerical study of breaking waves in the surf zone. Journal of Fluid Mechanics 359, 239-264.

Lin, P. and P. L. F. Liu (1998b). Turbulence transport, vorticity dynamics, and solute mixing under plunging breaking waves in surf zone. Journal of Geophysical Research 103, 15677-15694.

Lubin, P., S. Vincent, S. Abadie and J. P. Caltagirone (2006). Three-dimensional large eddy simulation of air entrainment under plunging breaking waves. Coastal Engineering 53, 631-655.

Lubin, P., S. Glockner, O. Kimmoun and H. Branger (2011). Numerical study of the hydrodynamics of regular waves breaking over a sloping beach. European Journal of Mechanics-B/Fluids 30(6), 552-564.

Peskin, C. S. and B. F. Printz (1993). Improved volume conservation in the computation of flows with immersed elastic boundaries. Journal of Computational Physics 105, 33-46.

Petit, H. A. H., P. Tonjes, M. R. A. van Gent and P. ven den Bosch (1994). Numerical simulation and validation of plunging breakers using a 2D Navier-Stokes model. Proceeding of 24th International Conference on Coastal Engineering, Kobe, ASCE, 511-524.

Ravoux, J. F., A. Nadim and H. Haj-Hariri (2003). An embedding method for bluff body flows: interactions of two side-by-side cylinder wakes. Theoretical and Computational Fluid Dynamics 16, 433-466.

Rodi, W. (1980). Turbulent models and their applications in hydraulics - a state of the art review. International Association for Hydraulic Research, Delft, 1-104.

Ting, F. C. K. and J. T. Kirby (1994). Observation of undertow and turbulence in a laboratory surf zone. Coastal Engineering 24, 51-80.

Tsai, C. Y., T. W. Hsu, S. H. Ou and Y. J. Jhu (2008). A 2D numerical simulation by VOF/PLIC method on wave breaking over a sloping bottom. Proceeding of 31th International Conference Coastal Engineering, Hamburg,

ASCE, 1-11.

Xie, Z. (2013). Two-phase flow modelling of spilling and plunging breaking waves. Applied Mathematical Modelling 37(6), 3698-3713.

Xie, Z. (2014). Numerical modelling of wind effects on breaking solitary waves. European Journal of Mechanics-B/Fluids 43, 135-147.

Zelt, J. A. (1991). The runup of nonbreaking and breaking solitary waves. Coastal Engineering 15, 205-246.

Zhao, Q., S. Armfield and K. Tanimoto (2004). Numerical simulation of breaking waves by a multi-scale turbulence model. Coastal Engineering 51, 53-80.

Zhao, Q. and K. Tanimoto (1998). Numerical simulation of breaking waves by large eddy simulation and VOF method. Proceeding of 26th International Conference Coastal Engineering, Copenhagen, ASCE, 892-905.